

THE DEVELOPMENT OF A KALMAN FILTER CLOCK PREDICTOR

J A Davis, C A Greenhall* and R Boudjemaa

National Physical Laboratory,
Hampton Road, Teddington, Middlesex, TW11 0LW

*Jet Propulsion Laboratory, California Institute of Technology,
4800 Oak Grove Dr. MS 298-100, Pasadena, CA 91109

ABSTRACT

A Kalman filter based clock predictor is developed, and its performance evaluated using both simulated and real data. The clock predictor is shown to possess a near to optimal Prediction Error Variance (PEV) when the underlying noise consists of one of the power law noise processes commonly encountered in time and frequency measurements. The predictor's performance in the presence of multiple noise processes is also examined. The relationship between the PEV obtained in the presence of multiple noise processes and those obtained for the individual component noise processes is examined. Comparisons are made with a simple linear clock predictor. The clock predictor is used to predict future values of the time offset between pairs of NPL's active hydrogen masers.

1. INTRODUCTION

National Measurement Institutes and Global Navigation Satellite System (GNSS) operators have both shown considerable interest in constructing atomic timescales that are maintained as close as possible to UTC. Because of the well-known latency in the publication of BIPM's Circular T, it is necessary to predict the future performance of an atomic timescale over periods of up to 50 days in order to maintain a local timescale that is close to UTC. Several authors have developed clock predictors. These range from the simple yet effective [1] to more elaborate designs for specific applications, e.g. GNSS [2].

Most clock predictors will provide a close to optimal prediction in the presence of a single well-specified noise process. The aim of the work described in this paper is to develop a clock predictor that will provide a close to optimal prediction in the presence of all noise processes commonly encountered in time and frequency measurements and in the presence of linear frequency drift. This is achieved by employing a two-stage analysis process. Initially, an adaptive Kalman filter is used to estimate the magnitude of the noise processes present within the clock measurements. The Kalman filter now possesses accurate noise parameters. This filter is then used to estimate the clock drift

parameters, from which predictions of the future clock offsets may be obtained.

A description of the noise processes encountered in atomic clocks and the approach used in this paper to model them is described in section 2. The design of the Kalman filter is described in section 3. The clock predictor's performance in the presence of both single and multiple noise processes is discussed in sections 4 and 5, respectively. The relationship between the Prediction Error Variance (PEV) obtained in the presence of multiple noise processes and those obtained for individual component noise processes is examined. The Kalman filter predictor's performance is compared directly against that of a simple linear predictor. An example of the application of the clock predictor is described in section 6, and concerns the prediction of future values of the time offset between pairs of NPL's active hydrogen maser.

An adaptive Kalman filter method has been employed to estimate the magnitude of the noise parameters. The method is based on the work of Meyer [3], the technique being modified and updated so as to estimate the noise parameters used in the clock models used in this paper. A detailed account of the noise parameter estimation method will be published shortly.

2. CLOCK NOISE AND DRIFT PARAMETERS

The noise processes occurring in atomic clocks and the associated measurement systems are traditionally modelled as a linear combination of five well known power law noise processes [4], these being White Phase Modulation (WPM), Flicker Phase Modulation (FPM), White Frequency Modulation (WFM), Flicker Frequency Modulation (FFM), and Random Walk Frequency Modulation (RWFM). An exact model of either FPM or FFM cannot be incorporated into a Kalman filter.

In this paper we describe the noise processes intermediate in structure between WPM and WFM and between WFM and RWFM as a linear combination of Markov and integrated Markov noise processes, respectively [5]. This model enables us to construct a good approximation to all FPM and FFM power law

noise processes intermediate in character between WPM and RWFM. In addition, we are able to describe noise processes observed in atomic clocks that are not well modelled as a linear combination of power law noise processes but may be described well using the Markov and integrated Markov noise processes.

The deterministic characteristics of atomic clocks may be described in terms of time offset, frequency offset, and in many situations linear frequency drift offset, drift parameters. In addition the relaxation "memory" associated with both the FPM and FFM noise processes is described approximately as a finite number of Markov drift parameters.

3. DESIGN OF THE CLOCK PREDICTOR

3.1 Kalman filter design

A clock predictor is used to estimate the future offsets between two clocks, using both current and previous measurements of the time difference. The Kalman filter clock predictor provides estimates of the deterministic parameters of the offset along with the PEV.

The clock predictor is implemented using the standard Kalman filter equations [6]. The measurements are assumed to be noiseless.

The state vector at measurement n is given by x_n where

$$x_n = (\xi_n, \eta_n, \zeta_n, m_{in}, \dots, m_{pn}, p_{in}, \dots, p_{pn})^T. \quad (3.1)$$

Here, ξ_n , η_n , and ζ_n are the time offset, frequency offset, and linear frequency drift offset components of the state vector, and m_{in} and p_{in} are the frequency and time offset of the i^{th} Markov frequency and phase components respectively.

The design matrix H is given by

$$H = (1, 0, 0, 0, \dots, 0, 1, \dots, 1). \quad (3.2)$$

The state propagation matrix Φ and process covariance matrix Q are based on equations (3.3) and (3.4) of [5]. The matrices described in [5] are extended to include components that operate on the Markov phase components of the state vector. The off-diagonal elements of these additional rows and columns are zero, and the vectors describing the diagonal elements are given by

$$\Phi_p = (\exp(-R_{p1}\tau_0) \dots \exp(-R_{pk}\tau_0))^T \quad (3.4)$$

and

$$Q_m = (\tau_0 a_{22}(R_{p1}\tau_0)\sigma_{p1}^2 \dots \tau_0 a_{22}(R_{pk}\tau_0)\sigma_{pk}^2)^T, \quad (3.5)$$

respectively, where R_{pi} is the time constant of the i^{th} Markov process, τ_0 is the spacing between successive measurements, and σ_{pi}^2 is the i^{th} Markov noise parameter.

3.2 Initialisation

To initialise the Kalman filter, the updated parameter covariance matrix P^+ is set to P_0^+ where P_0^+ contains only diagonal elements described by the vector T_0 where

$$T_0 = \left(\infty, \infty, \infty, \frac{\sigma_{m1}^2}{2R_{m1}}, \dots, \frac{\sigma_{mj}^2}{2R_{mj}}, \frac{\sigma_{p1}^2}{2R_{p1}}, \dots, \frac{\sigma_{pk}^2}{2R_{pk}} \right)^T. \quad (3.6)$$

The $T_{0\xi}$, $T_{0\eta}$ and $T_{0\zeta}$ components are set to very large values, and the T_{0mi} and T_{0pi} components are set to the "steady state" variances of the Markov processes. All elements of the state vector estimates \hat{x}_0^+ are set to zero.

In the situation where we are confident that linear frequency drift is not present in the clock measurements, e.g., in the long term comparisons of two caesium fountain clocks, then the ζ linear frequency drift parameter component of the state vector may be removed or alternatively $T_{0\zeta}$ is set to zero.

3.3 Prediction

To obtain a prediction of the clock offsets and the corresponding uncertainties we need to run the Kalman filter beyond the last available measurement y_c . The state vector estimates \hat{x}_δ^- , and parameter covariance matrix P_δ^- at prediction length δ are obtained using P_c^+ where

$$\hat{x}_\delta^- = \Phi(\delta)\hat{x}_c^+, \quad (3.7)$$

and

$$P_\delta^- = \Phi(\delta)P_c^+\Phi^T(\delta) + Q(\delta). \quad (3.8)$$

The time offset prediction \hat{y}_δ and the associated PEV V_δ^K are then given by

$$\hat{y}_\delta = H\hat{x}_\delta^- \quad (3.9)$$

and

$$V_\delta^K = HP_\delta^-H^T. \quad (3.10)$$

Combining equations (3.8) and (3.10) gives the following expression for the PEV:

$$V_\delta^K = H\Phi(\delta)P_c^+\Phi^T(\delta)H^T + HQ(\delta)H^T. \quad (3.11)$$

The first term on the right of equation (3.11) depends on the uncertainty in the extrapolation of the current estimate of the clock offset drift parameters, while the second term depends completely upon the stochastic processes occurring within the clocks.

4. PERFORMANCE IN THE PRESENCE OF A SINGLE NOISE PROCESS

4.1 Comparison with simple linear and optimal predictors

We compare the performance of the Kalman filter clock predictor against that of a simple linear predictor and where possible against that of an optimal clock predictor. The minimum possible PEV V^M has been previously calculated in the case of several power law noise processes from the power spectral density of those noise processes [1, 7]. Where possible we relate the PEV to the Allan variance $\sigma_y^2(\delta)$ of the noise process.

4.2 WFM Noise

In the presence of only WFM noise, assuming an infinite length data set and known linear frequency drift parameter, both the Kalman filter and simple linear clock predictors provide optimal predictions. This prediction is obtained from two infinitely spaced data points resulting in exact knowledge of the frequency offset parameter. The PEV and $\sigma_y^2(\delta)$ are then related by

$$V_{WFM}^M = \delta^2 \sigma_y^2(\delta) = \delta \sigma_{WFM}^2 \quad (4.1)$$

4.3 RWFM Noise

In the presence of RWFM noise and known linear frequency drift parameter, the optimal PEV is given by

$$V_{RWFM}^M = \delta^2 \sigma_y^2(\delta) = \frac{\delta^3}{3} \sigma_{RWFM}^2 \quad (4.2)$$

The PEV of the Kalman filter predictor is given by

$$V_{RWFM} = \frac{\delta^3}{3} \sigma_{RWFM}^2 + \delta^2 \sigma_{RWFM}^2 \frac{\tau_0}{\sqrt{12}} \quad (4.3)$$

The optimal PEV is only reached when we use infinitely small data spacing. This is due to the frequency offset parameter changing during the interval between the two measurements.

4.4 Single integrated Markov noise process

To study the performance of both the Kalman filter and simple linear predictor in the presence of FFM it is useful to determine the performance of these predictors in the presence of a single integrated Markov noise process. The relative performances of the two

predictors are shown in figure 1. The linear predictor is optimised at each prediction length δ .

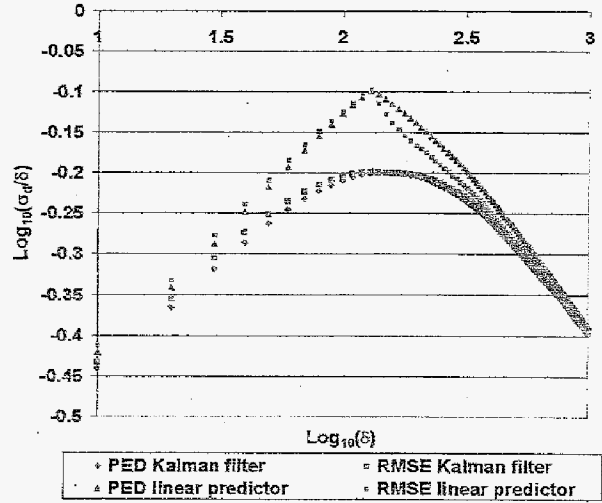


Figure 1 shows plots of $\text{Log}_{10}(\sigma_\delta/\delta)$, against $\text{Log}_{10}(\delta)$, obtained from the Kalman filter predictor (black and pink), and the simple linear predictor (blue and red), obtained both from theory (PED) and from simulations (RMSE) (2000 estimates).

Graphs of $\text{Log}_{10}(\sigma_\delta/\delta)$ against $\text{Log}_{10}(\delta)$ are plotted in figure 1, where σ_δ is the prediction error deviation. The results are presented in this form so that the gradients of the curves would be similar to, and hence easily compared with, graphs of $\text{Log}_{10}(\sigma_y(\delta))$ against $\text{Log}_{10}(\delta)$. The Prediction Error Deviation (PED) values obtained from theory and Room Mean Square Error (RSME) obtained from simulation agreed well.

A single Markov process is considered where $R = 1.18 \times 10^{-2} \text{ s}^{-1}$, $\tau_0 = 10 \text{ s}$, and the data length is ten times the maximum prediction length. The PEV was found to be lower in the case of the Kalman filter predictor at the "centre" of the Markov process. At long and short prediction lengths where the noise process resembles WFM and RWFM, respectively, the PEV values obtained from the two predictors were found to be similar.

5. PERFORMANCE IN THE PRESENCE OF MULTIPLE NOISE PROCESS

5.1 PEV inequality

The following inequality applies to the PEV obtained for a fixed δ when multiple noise processes are present:

$$V_{A+B}^M \geq V_A^M + V_B^M \quad (5.1)$$

where V_{A+B}^M is the minimum PEV for the sum $x_A(t) + x_B(t)$ of two independent noise processes, and V_A^M and V_B^M are the minimum PEV values obtained individually.

In previous literature [1, 7] the above inequality has been assumed to be an equality. While this may in some situations provide a reasonable approximation it may lead in many examples to significant errors in the PEV estimation.

To understand the origin of the above inequality we examine further equation (3.11). The second term on the right hand side of equation (3.11)

$$V^S = HQ(\delta)H^T \quad (5.2)$$

is the stochastic component of the PEV, its origin is due to noise occurring within the clock *after* the last measurement has occurred. When two or more noise processes are present this component of the PEV will add linearly.

The first term on the right hand side of equation (3.11)

$$V^D = H\Phi(\delta)P_c^+\Phi(\delta)^T H^T \quad (5.3)$$

gives the contribution to the Kalman filter PEV from uncertainties in the extrapolation of the drift parameters. The PEV inequality occurs within this "parameter extrapolation" term. When only the individual noise processes are present, the individual PEV values V_A and V_B are obtained using optimal values of the Kalman gain, K_A and K_B respectively. When we compute the PEV V_{A+B} from the combined noise processes we are using a different value K_{A+B} for the Kalman gain. In general the K_{A+B} value of the Kalman gain will not be the optimal Kalman gain when computing the PEV for either component noise process. Hence the resulting PEV V_{A+B} will be greater than the sum of the individual V_A and V_B PEV values and so leads to the inequality. If we used the same Kalman gain in all three cases the inequality would not occur, however the PEV values would then in most situations be sub-optimal.

5.2 Combination of WFM and RWFM noise processes

Consider the following example where there is a mixture of WFM and RWFM noise processes present with magnitudes σ_{WFM}^2 and σ_{RWFM}^2 . We assume an infinite data set so that the Kalman filter has reached a

steady state, and that the linear frequency drift term is either known or absent.

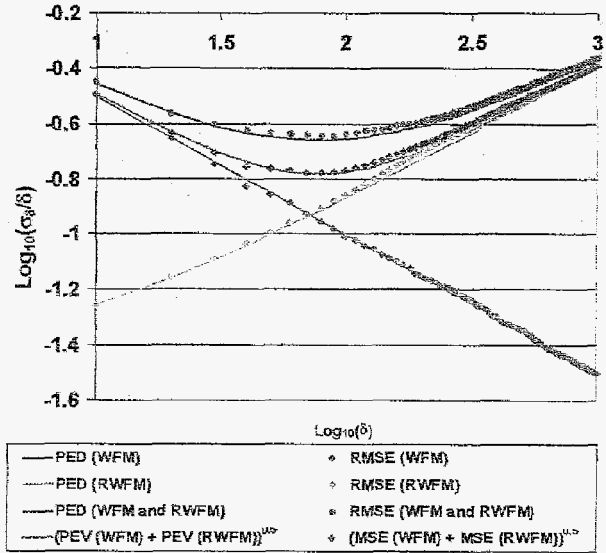


Figure 2 showing plots of $\text{Log}_{10}(\sigma_s/\delta)$ against $\text{Log}_{10}(\delta)$, obtained from the Kalman filter parameter covariance matrix (PED) and from simulation (RMSE) (500 estimates), in the case of WFM (pink), RWFM (green), a combination of WFM and RWFM (brown) and the sum of the individual noise process PEV values (blue).

The parameter covariance matrix then propagates according to the steady state Kalman filter equations

$$P^- = \Phi P^+ \Phi^T + Q \quad (5.4a)$$

$$K = P^- H^T (H P^- H^T)^{-1} \quad (5.4b)$$

$$P^+ = (I - KH)P^- \quad (5.4c)$$

where

$$\Phi = \begin{pmatrix} 1 & \tau_0 \\ 0 & 1 \end{pmatrix}, \quad (5.5)$$

and [8]

$$Q = \begin{pmatrix} \tau_0 \sigma_{WFM}^2 + \frac{\tau_0^3 \sigma_{RWFM}^2}{3} & \frac{\tau_0^2 \sigma_{RWFM}^2}{2} \\ \frac{\tau_0^2 \sigma_{RWFM}^2}{2} & \tau_0 \sigma_{RWFM}^2 \end{pmatrix}, \quad (5.6)$$

$H = (1 \ 0)$, and because the measurements are noiseless

$$P^+ = \begin{pmatrix} 0 & 0 \\ 0 & p \end{pmatrix}. \quad (5.7)$$

Solving the above simultaneous equations (5.4) for p and then substituting into equation (3.11) gives

$$V_s^k = \delta \sigma_{WPM}^2 + \frac{\delta^3}{3} \sigma_{RWPM}^2 + \delta^2 \sigma_{RWPM} (\sigma_{WPM}^2 + \frac{\tau_0^2}{12} \sigma_{RWPM}^2)^{1/2}. \quad (5.8)$$

The right hand term of (5.8) contains terms that include the multiplication of σ_{WPM} and σ_{RWPM} , the inequality given in equation (5.1) is clearly evident.

Comparing the brown and blue curves of figure 2 we observe that the PEV equality is clearly evident with the PEV values obtained from the combined noise processes (brown) possessing the higher PEV values.

5.3 Performance in the presence of FFM

FFM noise is present in active hydrogen masers. The optimal PEV obtained in the presence of a FFM noise process has been previously calculated [1, 7] as

$$V = \frac{\sigma_s^2 \delta^2}{\ln(2)}. \quad (5.9)$$

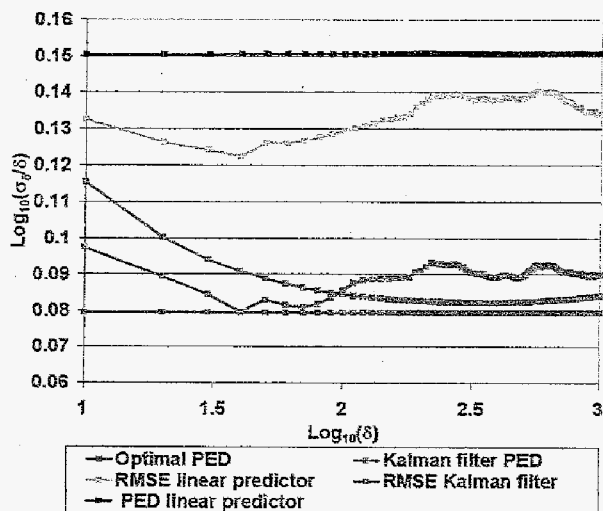


Figure 3 showing plots of $\text{Log}_{10}(\sigma_s / \delta)$ against $\text{Log}_{10}(\delta)$ obtained from the Kalman filter predictor (blue and pink), simple linear predictor (green and black), and from an optimal predictor (red); obtained both from theory (PED) and from simulations (RMSE) (2000 estimates).

The performance of both the Kalman filter and simple linear clock predictors in the presence of FFM and in the absence of linear frequency drift is shown in figure 3. These plots were obtained using simulated data and a data set that is ten times the maximum prediction length. The performance of the Kalman filter clock predictor is close to that of an optimal predictor, except at prediction lengths that are only a small multiple of the minimum data spacing τ_0 . In contrast, the simple linear predictor does not provide an optimal prediction. The best linear prediction was found to occur where the predictor point spacing was equivalent to the prediction length.

6. PREDICTOR EVALUATION USING REAL CLOCK AND TIME TRANSFER DATA

The performances of both the Kalman filter and simple linear predictors have been examined using 150 days of clock measurements made between NPL's three active hydrogen masers, with minimal spacing τ_0 of 600 s. The three pairs of clock differences were examined separately. The magnitude of the noise parameters were estimated as outlined in section 6 assuming that the clock noise may be described as a linear combination of integrated Markov noise processes. Clock predictions were made throughout the length of the data sets, and these were then compared against the actual clock data. The method was repeated using a simple linear predictor with optimal "point spacing".

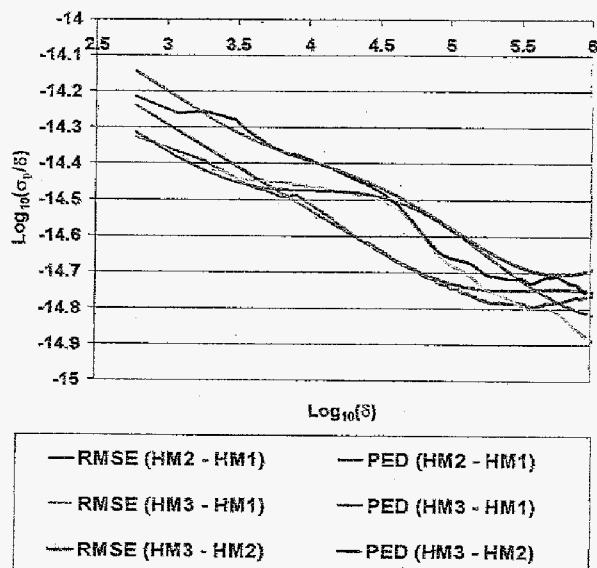


Figure 4 showing plots of $\text{Log}_{10}(\sigma_d / \delta)$ against $\text{Log}_{10}(\delta)$ for all three pairs of maser differences obtained from theory (PED) and simulation (RMSE) using the Kalman filter predictor.

Figure 4 plots of $\text{Log}_{10}(\sigma_d / \delta)$ against $\text{Log}_{10}(\delta)$ show that the RMSE obtained from the clock data and the PED estimates obtained from the Kalman filter agreed well at all prediction lengths. This helps confirm the validity of our model.

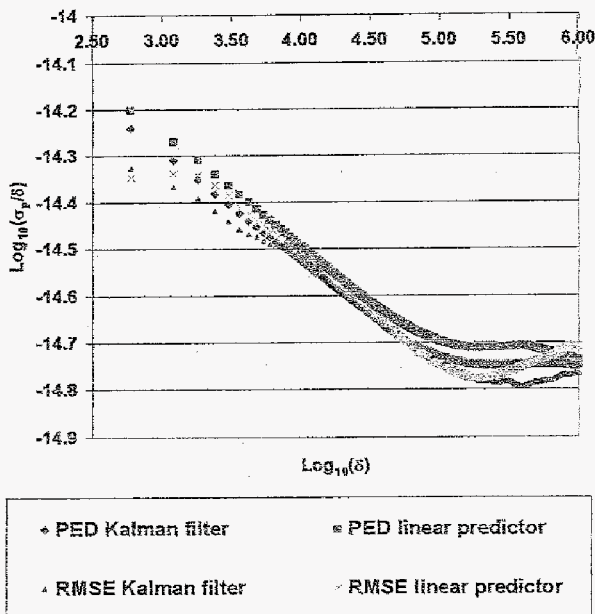


Figure 5 showing plots of $\text{Log}_{10}(\sigma_d/\delta)$ against $\text{Log}_{10}(\delta)$ for the (HM2-HM1) maser comparisons obtained from theory (PED) and simulation (RMSE) using both a Kalman filter and simple linear predictor.

Figure 5 shows the variation of PEV against prediction length for both the Kalman filter and simple linear predictor. The PEV and the root mean square prediction error agree well for both the Kalman filter and simple linear clock predictors. At all prediction lengths the theoretical PEV values are lower in the case of the Kalman filter clock predictor. The root mean square prediction errors obtained from the Kalman filter predictor are lower than those obtained from the linear predictor at most prediction lengths. At prediction lengths close to one day we observe that the root mean square prediction error obtained from the simple linear predictor is very slightly lower. One possible cause may be diurnal changes occurring within NPL's clock rooms, this may result in un-modelled periodic like effects perturbing the Kalman filter predictor.

8. CONCLUSIONS

A Kalman filter clock predictor has been developed. The performance of this predictor was found to be very close to optimal when operating on noise processes where the optimal PEV was known. The Kalman filter clock predictor performs significantly better than a simple linear predictor, in the presence of a single integrated Markov noise process, FFM noise and when used on NPL's hydrogen maser clock data.

The relationship between the PEV obtained in the presence of a single noise process and multiple noise process has been examined, and the magnitude of the PEV "inequality" examined.

9. ACKNOWLEDGEMENTS

The authors thank P W Stacey, R Hlavac and P B Whibberley for the provision of NPL's time scale data. This work has been supported by the Time and Frequency programme of the National Measurement System Policy Unit of the Department of Trade and Industry, UK. Part of the work was carried out at the Jet Propulsion Laboratory, California Institute of Technology, under a contract with the National Aeronautics and Space Administration.

REFERENCES

- [1] L-G Bernier, "Use of the Allan Deviation and Linear Prediction for the Determination of the Uncertainty on Time Calibrations Against Predicted Timescales". IEEE Trans. Instrumentation & Measurement, 52, no.2, 2003, p.483-486.
- [2] F Vernotte, Delporte J, M Brunet, and T Tournier, "Uncertainties of drift coefficients and extrapolation errors: Application to clock error prediction". Metrologia 2001, 38, no 4, 325-342
- [3] R K Mehra, "On the identification of variances and adaptive Kalman filtering". IEEE transactions on automatic control, AC-15, no 2, April 1970.
- [4] Handbook: selection and use of precise frequency and time systems, Chapter 3, International Telecommunication Union, 1997.
- [5] J A Davis, C A Greenhall, and P W Stacey, "A Kalman filter clock algorithm for use in the presence of flicker frequency modulation noise", Metrologia 42, 1-10, 2005.
- [6] R G Brown and Y C Hwang, "Introduction to random signals and applied Kalman filtering" third edition, John Wiley and Sons, 1997, chapter 5.
- [7] P Tavella and M Gotta, "Uncertainty and prediction of clock errors in space and ground applications". Proceedings of the 14th EFTF, 2000, pp 77-81 Turin.
- [8] S T Huttsell, "Relating the Hadamard variance to MSC Kalman filter clock estimation". Proceedings of the 14th Annual Precise Time and Time Interval (PTTI) Applications and Planning Meeting, 1995, pp 291-301.